PHOTONICS Research

Ultrabroadband microwave absorber based on 3D water microchannels

Yan Chen,[1] Kejian Chen,[1,*] Dajun Zhang,[2] Shihao Li,[1] Yeli Xu,[1] Xiong Wang,[2] and Songlin Zhuang[1]

[1]Shanghai Key Laboratory of Modern Optical System, Engineering Research Center of Optical Instrument and System, Ministry of Education, University of Shanghai for Science and Technology, Shanghai 200093, China
[2]School of Information Science and Technology, ShanghaiTech University, Shanghai 201210, China
*Corresponding author: ee.kjchen@gmail.com

Received 18 February 2021; revised 12 May 2021; accepted 12 May 2021; posted 13 May 2021 (Doc. ID 422686); published 1 July 2021

In this paper, an ultrathin and ultrabroadband metamaterial absorber based on 3D water microchannels is proposed. The experimental results show an absorption rate over 90% and a relative bandwidth up to 165% in the frequency band between 9.6 and 98.9 GHz. This polarization-independent absorber can work at a wide angle of incidence and exhibits good thermal stability. Benefiting from ultrabroadband absorption, thin thickness, low cost, and environmentally friendly materials, the proposed metamaterial absorber can be used in the fields of electromagnetic wave stealth and electromagnetic radiation protection. Related device design and research methods can be extended to the applied research in the terahertz and optical bands.

https://doi.org/10.1364/PRJ.422686

1. INTRODUCTION

Electromagnetic (EM) wave absorbers have been widely used in civil and homeland security applications for several decades, such as radar stealth [1], EM compatibility [2], energy harvesting [3], thermal emitters [4,5], and imaging systems [6,7]. With the rapid development of EM devices, research in recent years has mainly focused on making the absorber thinner and with a wider working bandwidth. However, traditional EM wave absorbers usually use high-loss materials such as ferromagnetic materials, which have inherent difficulties in reducing the volume and weight [8]. In recent years, the development of EM metamaterial absorbers (MMAs) has had a huge impact on traditional EM absorbers [9–14]. Among them, all-dielectric MMAs have shown unique potential in improving bandwidth and have become a new research hotspot. Water is a dielectric material that has the special characteristics of large permittivity and excellent dispersion characteristics [15], which give it high dielectric loss to electromagnetic waves in a wide frequency band. At the same time, water is liquid at room temperature, which makes it possible to construct flexible layouts. In 2015, Yoo *et al.* [16] first proposed the use of periodically arranged water droplets as a broadband MMA and achieved a broadband absorption of 8–18 GHz; in 2017, Peng *et al.* [17] proved that their water-based MMA has broadband and thermally adjustable absorption performance; in 2020, Zhang *et al.* [18] extended the absorption band edge to 9.3–49.0 GHz with a swastika-shaped water-based absorber.

In this paper, a 3D printed ultrathin and ultrabroadband water-based MMA is proposed. It can achieve an absorption rate over 90% in the band of 9.6–98.9 GHz, and the relative bandwidth is up to 165%. The experimental results prove the practicability of the absorber. In particular, the proposed absorber has the possibility of working at large incident angles and a weak dependence on the liquid's temperature range. Therefore, such absorber has great application value in the field of EM energy collection and EM stealth, especially in the navy field.

2. METHODS OF DESIGN, SIMULATION, AND EXPERIMENT

The proposed MMA is based on a 3D water microchannel, which is located inside a 3D printed polylactic acid (PLA) cube as shown in Fig. 1. The water microchannel of the absorber shown in Fig. 1(a) is composed of three layers. The bottom layer is composed of a cross water structure connected to an annular water channel. The length and width of the water channel cross are t_1 and t_2, respectively. The width of the bottom annular water microchannel is w_1. The middle layer, which is used to connect the top and bottom water structures, is a cross water microchannel structure too. The top layer is a square ring water microchannel with a width w_2 and length (the outer ring) l_2. The unit cell expands periodically in the x and y directions, and the period is p. The heights of

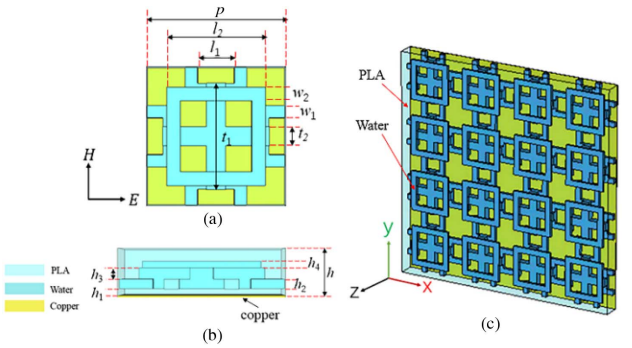

Fig. 1. (a) Unit of the water microchannel structure. (b) Side view of the unit. (c) Schematic of the metamaterial absorber.

the bottom, middle, and top water channels are h_2, h_3, and h_4, respectively, and the height of the PLA cube is h, which are shown in Fig. 1(b). The optimized structural parameters are set as $p = 10.1$ mm, $l_1 = 2.7$ mm, $l_2 = 7.2$ mm, $t_1 = 7.8$ mm, $t_2 = 1.4$ mm, $w_1 = 0.9$ mm, $w_2 = 1.0$ mm, $h_1 = 0.4$ mm, $h_2 = 0.6$ mm, $h_3 = 0.7$ mm, $h_4 = 0.4$ mm, and $h = 2.9$ mm. A 0.1 mm thick copper layer is attached on the back of the PLA cube, and the conductivity of copper is 5.96×107 S/m. The absorptivity in the simulation can be defined as $A = 1 - T - R = 1 - |S_{11}|^2 - |S_{21}|^2$, where T and R represent the transmissivity and reflectivity, respectively.

The simulation software CST Microwave Studio based on finite element analysis is used for numerical simulation. The cell boundary is adopted in the x and y directions, and the open boundary is adopted in the z direction. The incident EM wave is set to be polarized in the x direction and propagate in the $-z$ axis direction. The dielectric constant of PLA is set to 2.09, and the loss tangent is set to 0.07 [19]. The permittivity of pure water is represented by the Debye formula in the simulation [20]:

$$\varepsilon(\omega, T) = \varepsilon_\infty(T) + \frac{\varepsilon_s(T) - \varepsilon_\infty(T)}{1 - i\omega\tau(T)}, \tag{1}$$

where ε_s, ε_∞, and τ are the static permittivity, optical permittivity, and rotational relaxation time, respectively. Particularly, ε_s, ε_∞, and τ are all dependent on temperature as follows [20]:

$$\varepsilon_s(T) = a_1 - b_1 T + c_1 T^2 - d_1 T^3, \tag{2}$$

$$\varepsilon_\infty(T) = \varepsilon_s(T) - a_2 e^{-b_2 T}, \tag{3}$$

$$\tau(T) = c_2 e^{\frac{T_1}{T + T_0}}, \tag{4}$$

where $a_1 = 87.9$, $b_1 = 0.404\ \mathrm{K}^{-1}$, $c_1 = 9.59 \times 10^{-4}\ \mathrm{K}^{-2}$, $d_1 = 1.33 \times 10^{-6}\ \mathrm{K}^{-3}$, $a_2 = 80.7$, $b_2 = 4.42 \times 10^{-3}\ \mathrm{K}^{-1}$, $c_2 = 1.37 \times 10^{-13}$ s, $T_0 = 133$°C, $T_1 = 651$°C, and T (°C) is the temperature of water. Consequently, $\varepsilon_s = 78.4$, $\varepsilon_\infty = 3.1$, and $\tau = 8.27 \times 10^{-12}$ s are the parameters when water at room temperature $T = 25$°C. The absorption performance of the proposed absorber was studied and optimized at room temperature.

In order to qualitatively reveal the dissipation principle of the proposed water-based MMA, the influence of key structural parameters on its absorption performance is studied. As shown in Fig. 2(a), the changes of the width w_1 of the bottom annular water channel have almost no effect on the absorption performance. From Fig. 2(b), when the width of the square ring water channel on the top layer (w_2) expands from 0.5 to 2.0 mm, the intensity amplitude of the absorption peak changes by 12% near the frequency band at 30 GHz, and the stop band edge gradually shifts to the low frequency direction. When the thickness of the top square ring water channel increases, a similar phenomenon can also be observed as shown in Fig. 2(d). When the total thickness of the MMA remains unchanged, after scanning the thickness h_1 at the bottom of the PLA cube and the thickness h_4 of the top square ring water channel, it can be observed that the absorption intensity of the absorber changes greatly near the frequencies of 30 GHz and 70 GHz as shown in Figs. 2(c) and 2(d). In these two frequency bands, the absorption performance of the MMA is particularly sensitive to the changes in water structure parameters, which provides great flexibility for the design of the MMA.

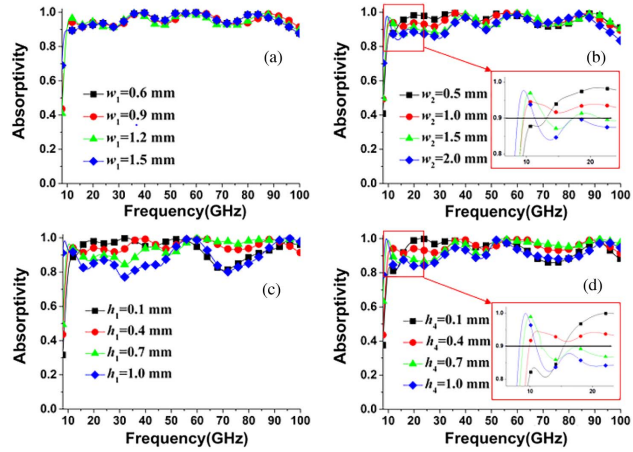

Fig. 2. Effect of changing structural parameters on absorption. (a) Width of bottom annular water channel. (b) Width of top square ring water channel. (c) Height of PLA bottom layer. (d) Height of top square ring water channel.

The fabricated absorber samples are made of PLA material by a fused deposition modeling (FDM) 3D printer, and the microchannel is filled with deionized (DI) water for packaging. Especially considering the narrow width of the water microchannel on the top and bottom layers, the water-absorbing calcium alginate hydrogel (add 2% w/v sodium alginate solution to 4% w/v calcium chloride solution) was filled during the printing process to solve the problem of bubbles which may exist in the water microchannel. This has almost no effect on the absorption performance of the absorber. The function of the designed microwave absorber is analyzed by a vector network analyzer (N5227A, Keysight Technologies) with broadband horn antennas at room temperature.

3. DISCUSSION OF SIMULATION AND EXPERIMENTAL RESULTS

In the frequency band of interest, the absorption rate of the entire PLA cube (Model_I in Fig. 3) is low at low frequencies and high at high frequencies. Inspired by the water channel

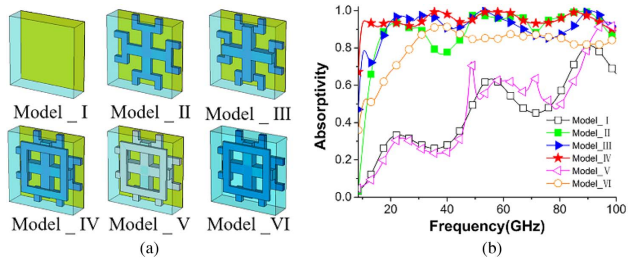

Fig. 3. (a) Unit cell of the designed devices, which are named Model_I, Model_II, Model_III, Model_IV, Model_V, and Model_VI. (b) Simulated absorptivity spectrum of different devices from Model_I to Model_VI.

resonator [21], the structure of Model_II is designed, which greatly improves the absorption performance and can reach 70% in the discussed frequency band. But the bandwidth where the absorption rate exceeds 90% is very narrow. To solve this problem, the cross channel in Model_II is extended, and Model_III is obtained. Then the bandwidth where the absorption rate exceeds 90% expands to 18.4–67.1 GHz. Furthermore, a square ring water channel is added on the top of the Model_III as shown in Model_IV in Fig. 3(a). An ultrabroadband microwave absorber based on a 3D water microchannel then can be achieved by the structure Model_IV. The frequency range where the absorption rate is higher than 90% is 9.6–98.9 GHz, and three absorption peaks can be observed at 37.00, 58.50, and 86.03 GHz. The absorption rates corresponding to these frequencies are 99.6%, 99.4%, and 99.1%, respectively. When the microchannel is not filled with water, as shown in Model_V, the absorption rate will drop sharply as shown by the purple hollow triangle line in Fig. 3(b). It means that the absorption performance of the device is mainly due to the specific water microstructure. In order to further analyze the absorption performance of the medium, the proposed device without a metal backplane (Model_VI) is also studied. It has a wider and better absorption rate compared with Model_I and Model_V, but its absorption intensity is greatly reduced compared with Models II to IV, especially at low frequencies, as shown in Fig. 3.

For further study, we have compared the different strategies of bandwidth enhancement and analyzed the mechanism of broadband absorption. The absorptivity and bandwidth can be increased by means of unit (Model_VI) stacking in the z direction as shown in Fig. 4(a), though the thickness needs to be sacrificed. On the other way, just a thin film metal sticks onto the back of the Model_VI structure, and a great bandwidth enhancement can be achieved. Fortunately, such metal layer can be the metal surface (mask) of any of the equipment or facilities.

Considering the mechanism of broadband absorption, the interference theory needs to be introduced first. Multiple reflections between the air–metamaterial interface and ground plane are illustrated in Fig. 4(b). At the interface between the air and the medium PLA, the incident microwave is partially reflected into the air and partially transmitted into the metamaterial structure, with the reflection coefficient $\tilde{r}_{21} = r_{21}e^{i\varnothing_{21}}$ and the transmission coefficient $\tilde{t}_{21} = t_{21}e^{i\theta_{21}}$. The latter continues

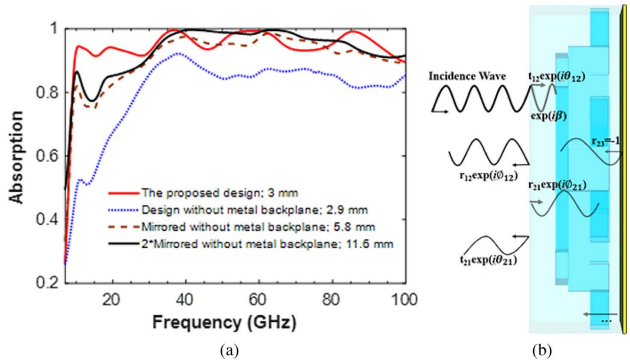

Fig. 4. (a) Strategies for improving absorption bandwidth. (b) The overview of the reflection and interference theory model.

to propagate to the metal ground surface, and there is a complex propagation phase $\tilde{\beta} = \beta_r + i\beta_i = \sqrt{\tilde{\varepsilon}_{\text{spacer}}}k_0 d$, where k_0 is the free-space wavenumber, β_r is the propagation phase, and β_i represents the absorption in the metamaterial structure. After multiple reflections and refractions, the overall reflection coefficient obtained is the superposition of multiple reflections [22]:

$$\tilde{r} = \tilde{r}_{12} - \frac{\tilde{t}_{12}\tilde{t}_{21}e^{i2\tilde{\beta}}}{1 + \tilde{r}_{21}e^{i2\tilde{\beta}}}. \tag{5}$$

The absorption of the device in a certain frequency range at normal incidence is calculated through multiple reflection theory to compare with the simulation results shown below. Although there is a slight difference between them, their absorption rates have the same trend, and the absorption intensity is basically consistent.

In order to further reveal the physical phenomenon behind the perfect absorption inside the metamaterial in higher frequency bands, whose wavelength is smaller than the unit size of the device, the power loss distribution of the MMA at three representative frequencies is studied. Power loss occurs in all parts of the water resonant cavity as shown in Fig. 5(a), which reflects that the power loss of the water-based MMA is mainly due to the strong dielectric loss of water. That is why the edge of the stop band moves to low frequencies when w_2 and h_4

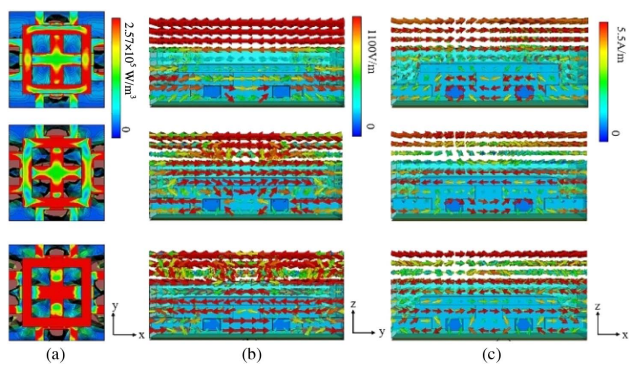

Fig. 5. Simulated vector distributions of (a) power loss densities, (b) electric fields, and (c) magnetic fields of the microwave absorber at 37.00 GHz (top), 58.50 GHz (middle), and 86.03 GHz (bottom).

become larger as shown in the insets of Figs. 2(b) and 2(d). From the perspective of effective media theory, as the dielectric constant of water is greater than that of PLA, the effective dielectric constant of the MMA will increase as the width (thickness) of the square annular water channel on the top layer increases, thereby increasing the effective electrical thickness, so the phenomenon of low-frequency redshift in Figs. 2(b) and 2(d) appears. In order to explore the absorption mechanism more deeply, the electric and magnetic field distributions of the MMA at three representative frequencies are simulated as shown in Figs. 5(b) and 5(c). At the first absorption peak 37.00 GHz, the electric field is mainly concentrated in the central PLA layer, and the magnetic field is mainly concentrated in the bottom water layer. This indicates that both strong electric resonance and strong magnetic resonance exist at this frequency. At the second absorption peak 58.50 GHz, the electric field is mainly concentrated in the entire water layer, and the magnetic field is mainly concentrated in the top water layer and the PLA contact layer. The third absorption peak is located at 86.03 GHz, with the same strong electric and magnetic resonance as the second absorption peak, and the electric and magnetic fields are distributed in similar positions and opposite directions. It is the synergy of these resonances that make the device able to achieve ultrabroadband absorption. Also, based on the impedance matching theory, we also can find evidence that the proposed absorber is able to achieve good absorption performance by matching its normalized surface impedance well with that of free space as shown in Fig. 6.

The absorption performance of our MMA has been experimentally studied by using five pairs of the standard broadband horn antennas (8–13, 12–18, 14.5–28, 22–45.4, 40–67, and 67–100 GHz). Each pair of antennas is connected to a vector network analyzer to measure the reflection coefficient and transmission coefficient of the subband. For instance, the inset of Fig. 7(b) shows a diagram of an experimental setup with a measurement frequency band of 22–45.4 GHz, which is the same as that setup used in Ref. [18]. The fabricated sample is shown in Fig. 7(a), where purple dye added is to better show the position of the water channel. The experimental curve confirms the ultrabroadband absorption performance, which is basically consistent with our simulation results, as shown in Fig. 7(b). Due to the deviation of the material parameters and the experimental system, it may cause slight differences between the experimental results and simulation results. But the experimental results can still prove the effectiveness of this absorber.

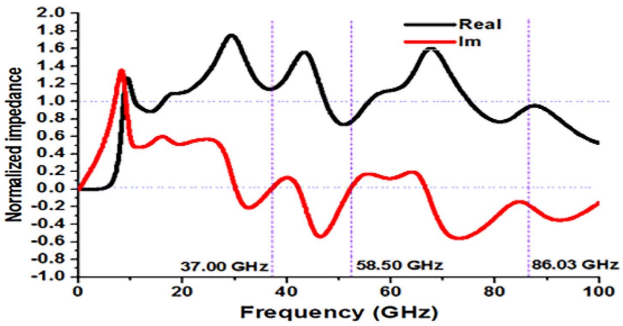

Fig. 6. Normalized impedance of the proposed device.

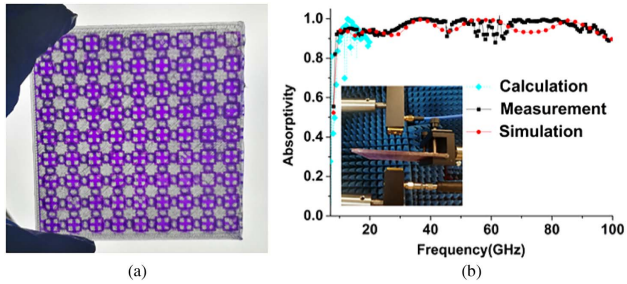

Fig. 7. (a) Fabricated sample; (b) comparison of the absorption spectra of calculated, measured, and simulated water MMA.

4. THERMAL STABILITY AND ANGULAR TOLERANCE

The temperature dependence of the dielectric constant of water raises concerns about the thermal stability of MMAs. In fact, as EM energy is converted into heat inside the metamaterial, the temperature of the water increases and maybe changes its absorption coefficient. In order to estimate the temperature

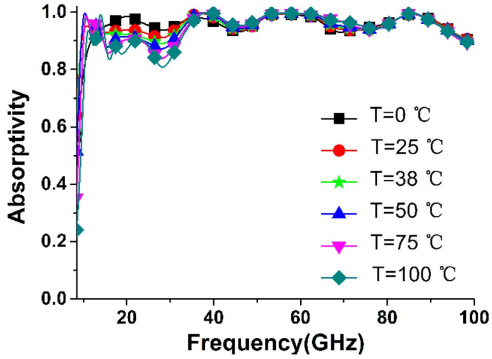

Fig. 8. Absorptivity spectra at different temperatures.

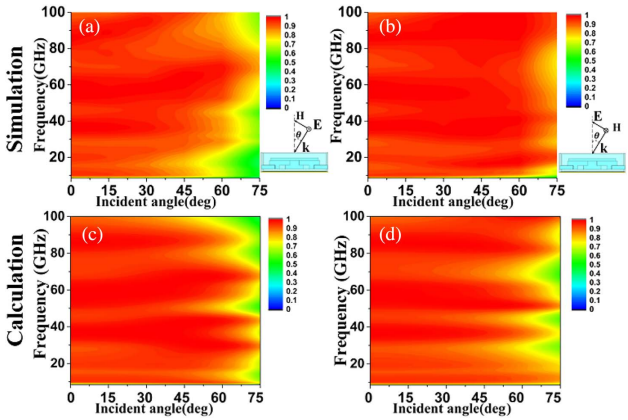

Fig. 9. Simulation and theoretical calculation of absorption spectra of water-based metamaterial absorbers with oblique incidence: (a), (c) TE mode; (b), (d) TM mode.

Table 1. Water-Based Absorbers Comparison

Ref.	Absorbers	Operating Band (GHz)	Relative Bandwidth (%)	Thickness (mm)	Relative Thickness (%)[a]	Experiment
[18]	Swastika-shaped	9.3–49.0	136	3.6	34.99	✓
[21]	All-dielectric	7.74–23.56	101	12.8	66.77	✓
[25]	Cylindrical water-based	5.58–24.10	125	5.6	27.70	✓
[26]	Round table	1.4–3.3	81	26.0	20.37	
		4.3–63.0	174		291.63	
[27]	Omnidirectional water-based	5.5–27.5	133	5.8	31.90	✓
[24]	Moth-eye structures	4–120	187	55	1136.7	
This work	3D water microchannel	9.6–98.9	165	3	54.25	✓

[a]Relative thickness is defined as $\mathrm{RT} = h/\lambda$, where h and λ represent the thickness and central wavelength ($\lambda = c/f$) of the device, respectively.

sensitivity of the MMA, the temperature dependence of the dielectric constant of water in the Debye formula is considered [20]. Figure 8 shows the absorptivity spectrum of the metamaterial in the temperature range from 0°C to 100°C. The curve shows that our structure is less sensitive to temperature in the frequency range of interest.

The absorption performance of the absorber under different incidence angles is further analyzed as shown in Fig. 9. From the simulation result as shown in Fig. 9(a), among the entire frequency band of interest, the absorption rate of TE waves decreases slightly as the incident angle increases. The absorption remains above 90% in almost the entire frequency band of interest when the incident angle is below 30°. Even if the incident angle is up to 45°, the absorption remains as high as 80%. For TM waves, when the incident angle is lower than 60°, the absorption exceeds 90%. As the incident angle of the TM-mode increases, the absorption spectrum of the absorber remains almost unchanged, which is similar to the typical changes of absorbers based on metal materials [23]. The difference in the absorption spectra under the polarization of TE and TM waves is mainly due to the difference in the magnetic field strength in the direction of the metamaterial surface. The absorption spectra of the TE wave and TM wave indicate that the proposed 3D water microchannel metamaterial absorber has good absorption performance for a wide range of incident angles.

In order to analyze the absorption trend of metamaterial absorbers at different incident angles more quantitatively with a theoretical model, the absorption rates in TE and TM modes were calculated according to Maxwell's equations [24], with the impedance retrieved from CST simulation results and the calculated effective permittivity (PLA: water = 7:3). It can be seen from Figs. 9(c) and 9(d) that the theoretical calculation results of Maxwell's equations are equivalent to the simulation results. Although a difference exists between them, they both show that the proposed absorber has practical angular tolerance for both incident polarizations.

In recent years, researchers have conducted extensive research on water-based absorbers and have proposed absorbers of various shapes. Table 1 lists the absorption bandwidth and thickness of water-based absorbers of different shapes. The table shows that the proposed absorber has both the widest bandwidth and the thinnest structural thickness.

5. CONCLUSION

In summary, the proposed 3D printed ultrathin and ultra-broadband water-based MMA can achieve more than 90% absorption in the range of 9.6–98.9 GHz, and the excellent absorption performance of the absorber is proved through experiments. It also shows that the proposed MMA can work under wide incident angles and exhibits good thermal stability and polarization-independent absorption performance. Such a kind of water-based metamaterial absorber has great application prospects in the field of EM energy harvest and stealth technology.

Funding. Shanghai Young College Teacher Development funding schemes (slg11006); National Natural Science Foundation of China (61205095).

Acknowledgment. We gratefully acknowledge Prof. H. Xiong from CQU and Dr. H. Kwon from U Texas for the discussion on the method of theoretical analysis.

Disclosures. The authors declare no conflicts of interest.

REFERENCES

1. E. F. Knott, J. F. Shaeffer, and M. T. Tuley, *Radar Cross Section*, 2nd ed. (SciTech Services, Inc., 2004).
2. D. D. L. Chung, "EM interference shielding effectiveness of carbon materials," Carbon **39**, 279–285 (2001).
3. T. S. Almoneef, F. Erkmen, and O. M. Ramahi, "Harvesting the energy of multi-polarized electromagnetic waves," Sci. Rep. **7**, 14656 (2017).
4. Z. Jiang, S. Yun, F. Toor, D. Werner, and T. S. Mayer, "Conformal dual-band near-perfectly absorbing mid-infrared metamaterial coating," ACS Nano **5**, 4641–4647 (2011).
5. A. K. Moridani, R. Zando, W. Xie, I. Howell, J. Watkins, and J. Lee, "Plasmonic thermal emitters for dynamically tunable infrared radiation," Adv. Opt. Mater. **5**, 1600993 (2017).
6. L. Lei, F. Lou, K. Tao, H. Huang, X. Cheng, and X. Ping, "Tunable and scalable broadband metamaterial absorber involving VO_2-based phase transition," Photon. Res. **7**, 734–741 (2019).
7. A. Tuniz, K. J. Kaltenecker, B. M. Fischer, M. Walther, S. C. Fleming, A. Argyros, and B. T. Kuhlmey, "Metamaterial fibres for subdiffraction imaging and focusing at terahertz frequencies over optically long distances," Nat. Commun. **4**, 2706 (2013).
8. J. L. Wallace, "Broadband magnetic microwave absorbers: fundamental limitations," IEEE Trans. Magn. **29**, 4209–4214 (1993).
9. N. I. Landy, S. Sajuyigbe, J. J. Mock, D. R. Smith, and W. J. Padilla, "Perfect metamaterial absorber," Phys. Rev. Lett. **100**, 207402 (2008).

10. Y. Pang, J. Wang, H. Ma, M. Feng, Y. Li, Z. Xu, S. Xia, and S. Qu, "Spatial k-dispersion engineering of spoof surface plasmon polaritons for customized absorption," Sci. Rep. **6**, 29429 (2016).
11. Y. Cui, K. H. Fung, J. Xu, H. Ma, Y. Jin, S. He, and N. X. Fang, "Ultrabroadband light absorption by a sawtooth anisotropic metamaterial slab," Nano Lett. **12**, 1443–1447 (2012).
12. B. Zhu, Z. Wang, C. Huang, Y. Feng, J. Zhao, and T. Jiang, "Polarization insensitive metamaterial absorber with wide incident angle," Prog. Electromagn. Res. **101**, 231–239 (2010).
13. C. Zhang, J. Yang, W. Cao, W. Yuan, J. Ke, L. Yang, Q. Cheng, and T. Cui, "Transparently curved metamaterial with broadband millimeter wave absorption," Photon. Res. **7**, 478–485 (2019).
14. J. Zhao, S. Wei, C. Wang, K. Chen, B. Zhu, T. Jiang, and Y. Feng, "Broadband microwave absorption utilizing water-based metamaterial structures," Opt. Express **26**, 8522–8531 (2018).
15. A. Andryieuski, S. Kuznetsova, S. Zhukovsky, Y. Kivshar, and A. Lavrinenko, "Water: promising opportunities for tunable all-dielectric electromagnetic metamaterials," Sci. Rep. **5**, 13535 (2015).
16. Y. J. Yoo, S. Ju, S. Y. Park, Y. J. Kim, J. Bong, T. Lim, K. W. Kim, J. Y. Rhee, and Y. P. Lee, "Metamaterial absorber for electromagnetic waves in periodic water droplets," Sci. Rep. **5**, 14018 (2015).
17. Y. Pang, J. Wang, Q. Cheng, S. Xia, and S. Qu, "Thermally tunable water-substrate broadband metamaterial absorbers," Appl. Phys. Lett. **110**, 104103 (2017).
18. X. Zhang, D. Zhang, Y. Fu, S. Li, Y. Wei, K. Chen, X. Wang, and S. Zhuang, "3D printed swastika shape ultra-broadband water-based microwave absorber," IEEE Antennas Wireless Propag. Lett. **19**, 821–825 (2020).
19. Y. Youngseo, L. Daecheon, M. M. Tentzeris, and L. Sungjoon, "Low-cost metamaterial absorber using three-dimensional circular truncated cone," Microw. Opt. Technol. Lett. **60**, 1622–1630 (2018).
20. W. J. Ellison, "Permittivity of pure water, at standard atmospheric pressure, over the frequency range 0–25 THz and the temperature range 0–100°C," J. Phys. Chem. Ref. Data **36**, 1–18 (2007).
21. J. Xie, S. Quader, F. Xiao, C. He, and I. D. Rukhlenko, "Truly all-dielectric ultra-broadband metamaterial absorber: water-based and ground-free," IEEE Antennas Wireless Propag. **18**, 536–540 (2019).
22. H. T. Chen, "Interference theory of metamaterial perfect absorbers," Opt. Express **20**, 7165–7172 (2012).
23. H. Tao, C. M. Bingham, A. C. Strikwerda, D. Pilon, D. Shrekenhamer, N. I. Landy, K. Fan, X. Zhang, W. J. Padilla, and R. D. Averitt, "Highly flexible wide angle of incidence terahertz metamaterial absorber: design, fabrication, and characterization," Phys. Rev. B **78**, 241103 (2008).
24. H. Kwon, G. D'Aguanno, and A. Alu, "Optically transparent microwave absorber based on water-based moth-eye structures," Opt. Express **29**, 9190–9198 (2021).
25. R. Jian and Y. Yuan, "Cylindrical-water-resonator-based ultra-broadband microwave absorber," Opt. Mater. Express **8**, 2060–2071 (2018).
26. H. Xiong and F. Yang, "Ultra-broadband and tunable saline water-based absorber in microwave regime," Opt. Express **28**, 5306–5316 (2020).
27. Y. Zhou, Z. Shen, J. Wu, Y. Zhang, S. Huang, and H. Yang, "Design of ultra-wideband and near-unity absorption water-based metamaterial absorber," Appl. Phys. A **126**, 52 (2020).